Steel and Composite Structures, *Vol. 17, No. 4 (2014) 431-452*
DOI: http://dx.doi.org/10.12989/scs.2014.17.4.431

Mechanical behaviour of concrete filled double skin steel tubular stub columns confined by FRP under axial compression

Jun Wang *, Weiqing Liu, Ding Zhou, Lu Zhu and Hai Fang

College of Civil Engineering, Nanjing Tech University, Nanjing 211816, People's Republic of China

(*Received July 16, 2012, Revised March 11, 2014, Accepted March 18, 2014*)

Abstract. The present study focuses on the mechanical behaviour of concrete filled double skin steel tubular (CFDST) stub columns confined by fiber reinforced polymer (FRP). A series of axial compression tests have been conducted on two CFDST stub columns, eight CFDST stub columns confined by FRP and a concrete-filled steel tubular (CFST) stub column confined by FRP, respectively. The influences of hollow section ratio, FRP wall thickness and fibre longitudinal-circumferential proportion on the load-strain curve and the concrete stress-strain curve for stub columns with annular section were discussed. The test results displayed that the FRP jacket can obviously enhance the carrying capacity of stub columns. Based on the test results, a new model which includes the effects of confinement factor, hollow section ratio and lateral confining pressure of the outer steel tube was proposed to calculate the compressive strength of confined concrete. Using the present concrete strength model, the formula to predict the carrying capacity of CFDST stub columns confined by FRP was derived. The theoretically predicted results agree well with those obtained from the experiments and FE analysis. The present method is also adapted to calculate the carrying capacity of CFST stub columns confined by FRP.

Keywords: FRP; concrete filled steel tubular column; double skin; axial compression

1. Introduction

Concrete-filled steel tubular (CFST) columns have found increasingly wide applications in civil engineering. By filling the steel hollow section with concrete, the failure of the steel tube due to buckling could be delayed and the strength and ductility of the concrete core could be improved significantly as a result of the confinement of the steel tube (Furlong 1967, Knowles and Park 1969). As a new kind of CFST constructions, a concrete-filled double skin steel tubular (CFDST) column consists of two concentric steel tubes with concrete sandwiched between them. CFDST columns were firstly introduced into the vessel design to resist external pressure (Montague 1978). They have almost the same advantages in traditional CFST columns. However, they have lighter weight, higher bending stiffness, and better cyclic performance than the CFST columns (Nie and Liao 2008, Han *et al.* 2009 and Tao *et al.* 2004). Along with the advantages of this type of structure columns, come the drawbacks associated to the susceptibility of steel to environment chemical, electrochemical or physical materials, which could result in corrosion and weaken the

*Corresponding author, Associate Professor, E-mail: wangjun3312@njtech.edu.cn

http://www.techno-press.org/?journal=scs&subpage=8 ISSN: 1229-9367 (Print), 1598-6233 (Online)

mechanical properties of steel. To overcome the existing disadvantages in CFST and CFDST columns, using FRP jacket as an external means to strengthen steel tubes appears to be an excellent approach. Recent experiences in USA, UK, Japan and Switzerland displayed that there is a great potential in using FRP to retrofit steel structures (Zhao and Zhang 2007). Using glass FRP (GFRP) to protect corrosion of steel structures has been codified by Ministry of Transport of the People's Republic of China (JTS 153-3-2007).

The existing applications on FRP-to-steel composites are mainly in the repair of structures (Seica and Packer 2007). One of the early studies on this topic involved the use of carbon FRP (CFRP) laminates in repairing of steel-concrete composite bridge sections (Sen and Liby 1994). Tao *et al.* (2007, 2008) carried out monotonic and cyclic tests on fire-exposed CFST elements such as columns, beams and beam-columns repaired with CFRP wraps. They demonstrated that FRP composites were effective in enhancing the carrying capacity of columns and beam-columns while the strengthening effect on beams was quite limited if only unidirectional FRP was used to confine the beams. Park *et al.* (2011) compared the structural behaviors of CFRP reinforced columns with those of CFST columns. The tests results indicated that using CFRP to confine CFST columns could significantly increase the axial carrying capacity due to the additional confinement effect by FRP. However, ductility capacity was consequently decreased because of the sudden rupturing of FRP. Three mono-poles strengthened by several configurations of CFRP were tested as cantilevers (Schnerch and Rizkalla 2004). As a result, the stiffness increased from 17% to 53%, which demonstrated the adequacy of the employed strengthening method. Wang *et al.* (2005a, b) analyzed the influence of steel and CFRP tube confinement coefficients on carrying capacity of the concentrically compressed CFST columns confined by CFRP. They proposed a simple formula to estimate the carrying capacity of concentrically concrete filled in CFRP-steel composite tubular stub columns.

In addition, using FRP to strengthen hollow steel tubes has attracted a significant amount of attention. An analytical approach for calculating ultimate strength of composite steel-carbon fibre reinforced beams was presented by Haedir *et al.* (2010). Teng and Hu (2007) carried out a series of axial compression tests to study the effectiveness of FRP confinement on steel tubes. They found that the column ductility was enhanced because the FRP confinement controlled the development of the elephant's foot buckling mode. Shaat and Fam (2006) tested the short and long columns with square hollow steel section, strengthened by CFRP under axial loading. A strength increase of 18% was achieved for the short columns with two transverse CFRP layers, while the strength increase for the long columns was highly dependent on the column's imperfection. Nishino and Furukawa (2003) found that the carbon fiber reinforcement can improve the deformation and seismic performance of steel tube beam-columns. Seica and Packer (2007) discussed the suitability of FRP in repairing tubular steel members and the structural behavior under marine environment. They found that the composite members wrapped and cured underwater were not able to attain the flexural capacity as they were cured in air. Jiao and Zhao (2004) studied the circular hollow section members subjected to tension and confined by CFRP sheets. As described by Jiao and Zhao (2004), the most effective reinforcing scheme is to identify a suitable epoxy as well as an effective bond length of the connected composite fibres.

Over the past few decades, the researches on strengthening of CFST columns preliminarily demonstrated the effectiveness of CFRP wraps in increasing the axial carrying capacity of CFST columns. However, no research concerning with the effectiveness of CFDST columns wrapped by FRP composites has been conducted so far. The CFDST columns confined by FRP have the following advantages: (a) the lightweight and corrosion resistance; (b) the ability of the inner steel

tube to bear construction load; (c) better confinement of concrete. It is well known that unlike glass, carbon is an electrical conductor, therefore galvanic corrosion could take place if fibres contact directly with metals (Miller *et al.* 2001).

The paper studies the axial behaviour of CFSDT stub columns confined by FRP where both inner steel tube and outer steel tube have the hollow sections. The axial tests have been conducted on eight CFDST stub columns confined by FRP. The tests for two CFDST stub columns and a CFST column confined by FRP were also conducted for the comparison. The main parameters used in the stub column tests are: (1) hollow section ratios: 0.47 and 0.71; (2) FRP wall thicknesses: 0.9 mm, 2.7 mm and 4.5 mm; (3) fibre longitudinal- circumferential proportions: 1:1, 1:2 and 1:4. When one parameter was studied, the other parameters were kept constants. The simplified model was presented to predict the strength of confined concrete. Based on the simplified model, the theoretical formula to calculate the carrying capacity of the composite columns was derived out.

2. Experimental investigation

The cross section of CFSDT stub columns confined by FRP where both inner and outer steel tubes have hollow sections is shown in Fig. 1. The space between two steel tubes was filled with concrete. A series of axial compression tests were conducted to study the influences of hollow section ratio, FRP wall thickness and fibre longitudinal- circumferential proportion on load-strain curves and concrete stress-strain curves of the stub columns with annular section, confined by FRP.

2.1 Specimen for test

Eight specimens of CFDST stub columns confined by FRP were prepared for test, which have the same height of 500 mm and the same outer steel tube wrapped with GFRP sheet. The surface of the outer steel tube was cleaned. First, the outer steel tube was applied by a layer of resin then it was continuously wrapped by a layer of bidirectional glass sheet. Similarly, the second layer of the resin was applied to the bidirectional glass sheet and then it was wrapped by a layer of bidirectional glass sheet and so on. After the last layer of laminate was wrapped, a surface layer of resin was further applied. The 50 mm length at the top and bottom of the column was reinforced with

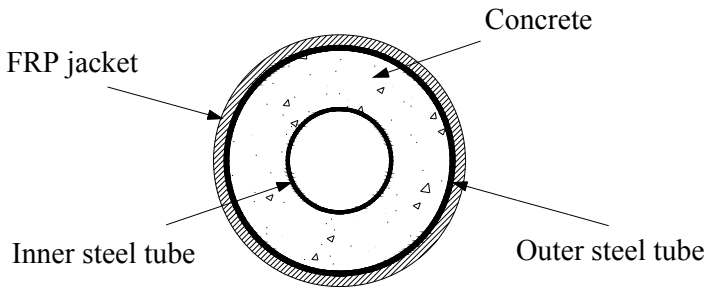

Fig. 1 Typical section of CFDST column confined by FRP

three layers of GFRP to avoid the splitting of the head during loading. Moreover, two CFDST stub columns and a CFST column confined by FRP were also fabricated to observe the differences of their behaviour with CFDST stub columns confined by FRP. The specimen parameters were described by hollow section ratio K_v, thickness of FRP jacket and fibre longitudinal-circumferential proportion.

The hollow section ratio is defined as

$$K_v = \frac{D_i}{D_o - 2t_{s1}} \tag{1}$$

where D_o and D_i are outside diameters of the outer and inner steel tubes, respectively; t_{s1} is the wall thickness of the outer steel tube.

The dimensions of the specimens are given in Table 1, where t_f and t_{s2} are the wall thicknesses of FRP jacket and inner steel tube, respectively.

2.2 Material properties

The FRP laminates were applied directly to the pretreated surfaces of the outer steel tubes to provide lateral confinement in the hoop direction. E-glass/epoxy jackets were used to confine the column. The fibre longitudinal-circumferential proportion was taken as 1:1, 1:2 and 1:4, respectively. To determine the material properties of the FRP, three flat and three circle coupon tests were conducted for each fibre proportion. Table 2 presents the measured properties of the composite materials used.

Table 1 Dimensions of specimens for the test

Specimen[a]	t_f (mm)	Fibre longitudinal- circumferential proportion	K_v	D_o (mm)	t_{s1} (mm)	D_i (mm)	t_{s2} (mm)
3SA4	2.7	1:4	—	165	1.7	—	—
0HA0	0	—	0.47	165	1.7	76	1.2
1HA4	0.9	1:4	0.47	165	1.7	76	1.2
3HA4	2.7	1:4	0.47	165	1.7	76	1.2
3HA2	2.7	1:2	0.47	165	1.7	76	1.2
3HA1	2.7	1:1	0.47	165	1.7	76	1.2
5HA4	4.5	1:4	0.47	165	1.7	76	1.2
0HB0	0	—	0.71	165	1.7	114	1.7
1HB4	0.9	1:4	0.71	165	1.7	114	1.7
3HB4	2.7	1:4	0.71	165	1.7	114	1.7
5HB4	4.5	1:4	0.71	165	1.7	114	1.7

[a] In the first column, the first number means fibre layers and the last number means fibre longitudinal-circumferential proportion, the letter *S* means solid column and the letter *H* means hollow column, the letter *A* means the hollow section ratio of specimen 0.47 and the letter *B* means the hollow section ratio of specimen 0.71.

Notes: t_f is the wall thickness of FRP jacket, K_v is the hollow section ratio, D_o is the outside diameter of outer steel tube, D_i is the outside diameter of inner steel tube, t_{s1} is the wall thickness of outer steel tube and t_{s2} is the wall thickness of inner steel tube.

Table 2 Mechanical properties of GFRP jackets

Fibre longitudinal-circumferential proportion	Tensile properties				Compressive properties		
	Lateral strength (MPa)	Axial strength (MPa)	Lateral modulus (GPa)	Axial modulus (GPa)	Axial strength (MPa)	Axial modulus (GPa)	Poisson ratio
1:1	299.66	299.66	22.73	22.73	37.46	9.37	0.194
1:2	328.57	212.99	22.80	15.71	35.84	8.80	0.223
1:4	460.03	74.96	24.50	7.36	35.84	5.76	0.220

Cold-formed circular steel tubes were used in the construction of the specimens. Standard tensile coupon tests were conducted to measure the material properties of the steel tubes. 0.2% proof stress was adopted as the yield stress. The tests show that both outer steel tube and inner steel tube have a yield stress of 350 MPa and a Young's modulus of 190.53 GPa.

All the specimens used the concrete of the same batch. Three 150 mm cubes were cast and cured under the conditions similar to the related specimens. The average cube compressive strength at 28 days was 28.05 MPa.

2.3 Test set-up and instrumentation

A universal testing machine with 2000 kN capacity was used for compression tests on all specimens. The axial load was applied through a very stiff top platen, and an endplate was welded on the steel tubes. The endplate and the top platen were made of high strength steel with a thickness of 20 mm.

For each CFDST column specimen confined by FRP, four bi-directional strain rosettes (gauge length 10 mm) were placed at 90° apart on the middle of outer and inner surfaces of the column, respectively. In addition, eight linear variable displacement transducers (LVDTs) were used to measure the axial strain of the column at the top and the end of the specimen during test. The strain gauges and displacement meters were put with reference to Fig. 2. The testing for CFST confined by FRP was only made on the outer surface of the columns.

A load interval within one tenth of the estimated carrying capacity was taken, and each load interval was maintained for 2 to 3 minutes in the test. At each load increment, the strain and the deflection were recorded. All the specimens were loaded up to failure.

2.4 Test results and discussions

2.4.1 Overall observations

All the specimens displayed continuous load-displacement behavior until ultimate failures except the specimen 5HB4 for which, the failure came from the initial loading eccentricity. During the initial loading stage, in general the axial load is approximately proportional to the axial strain. There is no obvious change in the appearance of the specimens.

Consider the specimens with hollow section ratio 0.47. For the specimen without FRP (0HA0), the local buckling occurred in the middle of the outer steel tube when the load attained 70% of the ultimate load. As the load increased further, the outward deformation around the circumference dominated the behaviour of the outer steel tube, and the elephant's foot bucking mode near the

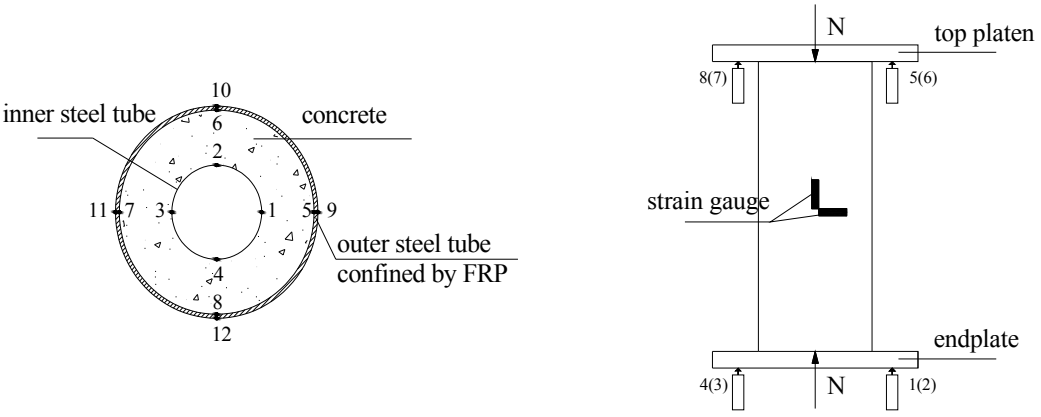

Fig. 2 The layout of strain gauges and displacement meters: (a) Strain gauge arrangement on middle cross-section; (b) Elevation of displacement meter arrangement, (the number in parentheses means the displacement meters in another side)

tube end appeared. In contrast, the failure of specimens with FRP (1HA4, 3HA4 and 5HA4) involved the rupture of the FRP jacket due to the expanding local buckling deformation. The hoop crack on the FRP was initiated when the load attained 50% of the ultimate load. The appearance of the new cracks and the extension of existed cracks were observed upon the further loading. It is obvious that for specimens with FRP, the hoop deformation were accordingly increased as the thickness of the FRP jacket increased. When the compression tests finished, it was observed that the inner steel tubes had inward buckling deformations. The four specimens after failure are shown in Fig. 3.

When the hollow section ratio changed to 0.71, the failure modes of specimens were similar to those with hollow section ratio 0.47. This means that the change of the hollow ratio only affects the carrying capacities of the CFDST stub columns wrapped by FRP, but has no significant influence on their failure behaviour. For the solid specimen 3S4, the more local ruptures

Fig. 3 Failures of specimens with different FRP jacket thicknesses (a) 0HA0; (b) 1HA4; (c) 3HA4; (d) 5HA4

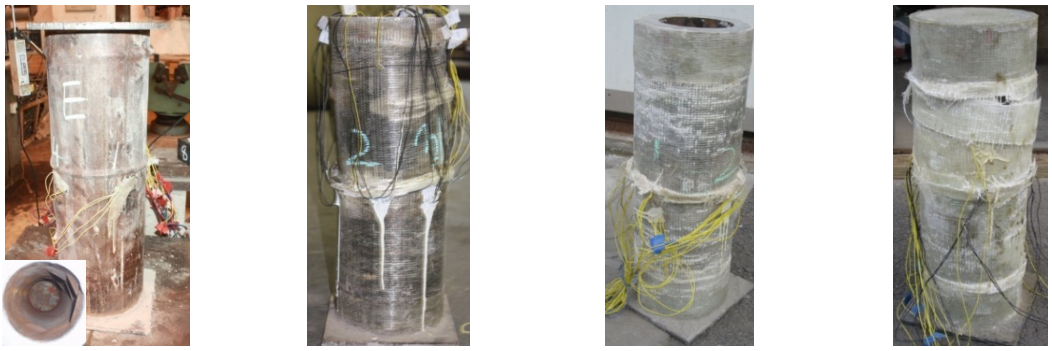

(a) (b) (c) (d)

Fig. 4 Failures of specimens with different hollow ratios: (a) 0HB0; (b) 1HB4; (c) 3HB4; (d) 3SA4

(a) (b)

Fig. 5 Failures of specimens with different fibre longitudinal-circumferential proportions: (a) 3HA2; (b) 3HA1

occurred along the FRP jacket. Typical failure appearances of specimens 0HB0, 1HB4, 3HB4 and 3SA4 are shown in Fig. 4.

In addition, for specimens with fibre longitudinal-circumferential proportion 1:1 (3HA1) and 1:2 (3HA2), it was observed that a block of FRP near the mid-height of specimen was ruptured. The failure of specimens 3HA1 and 3HA2 was more sudden than that of specimen 3HA4 which has the fibre longitudinal-circumferential proportion 1:4. This means that the circumferential FRP can effectively delay the local buckling of the outer steel tube, as observed by Tao et al. (2007). The failure appearances of specimens 3HA1 and 3HA2 are shown in Fig. 5.

2.4.2 Behavior of composite columns

The carrying capacity $N^*_{u,fs}$ obtained from the test is summarized in Table 3, where a confinement factor ζ is defined to describe the composite relationship among FRP jacket, outer steel tube and concrete as follows

$$\zeta = \zeta_f + \zeta_s \tag{2}$$

Table 3 Confinement factors and carrying capacities

Specimen	ξ_f	ξ_s	Ξ	$N^*_{u,fs}$ [a] (kN)
3SA4	1.70	0.79	2.49	1820
0HA0	0	1.02	1.02	980
1HA4	0.72	1.02	1.74	1160
3HA4	2.18	1.02	3.20	1420
3HA2	1.56	1.02	2.58	1400
3HA1	1.42	1.02	2.44	1332
5HA4	3.67	1.02	4.69	1870
0HB0	0	1.58	1.58	715
1HB4	1.12	1.58	2.70	776
3HB4	3.38	1.58	4.96	1040
5HB4	5.69	1.58	7.27	1020

[a] $N^*_{u,fs}$ is the carrying capacities obtained from the experiment.
Notes: ζ_f is the confinement factor of FRP jacket, ζ_s is the confinement factor of outer steel tube, $\zeta = \zeta_f + \zeta_s$.

$$\zeta_f = A_f f_f / A_c f'_{co} \tag{3}$$

$$\zeta_s = A_{s1} f_{yo} / A_c f'_{co} \tag{4}$$

In which, ζ_f is the confinement factor of FRP jacket, ζ_s is the confinement factor of outer steel tube, A_f is the cross-sectional area of FRP jacket, A_c is the cross-sectional area of concrete, A_{s1} is the cross-sectional area of outer steel tube, f_f is the tensile strength of FRP jacket, f_{yo} is the yield strength of outer steel tube and f'_{co} is the compression strength of unconfined concrete. The value of f'_{co} is taken as 67% of the compression strength of the cubic blocks.

The enhancements of axial carrying capacity of CFDST stub columns due to the FRP wrapping can be gauged using the strengthening ratio, which is defined as the percentage increase in the carrying capacity

$$SEI = \left(N_{u,fs} - N_{u,s}\right) / N_{u,s} \times 100\% \tag{5}$$

where $N_{u,fs}$ is the carrying capacity of CFDST stub column confined by FRP, and $N_{u,s}$ is the carrying capacity of CFDST stub column. It could be seen from Fig. 6 that the higher the confinement factor (ζ), the higher the carrying capacity (SEI).

Load versus axial strain measured from the specimens with different FRP wall thicknesses (i.e., 0HA0, 1HA4, 3HA4 and 5HA4) are plotted in Fig. 7(a), where the strains were recorded by the displacement transducer readings. The axial stress-strain curves of the concrete in these specimens are shown in Fig. 7(b), where the axial stresses in the concrete were determined through dividing the load on the concrete by the cross-sectional area of the concrete. The load carried by the concrete was defined as that of the load carried by the specimen minus the loads carried by the FRP jacket and the outer and inner steel tubes under the same axial strain, as described by Teng *et al.* (2007). It could be seen from Fig. 7(a) that the specimen 0HA0 ($t_f = 0$) has an almost elastic-perfectly plastic load-stain curve, while the specimens wrapped with FRP have a bilinear

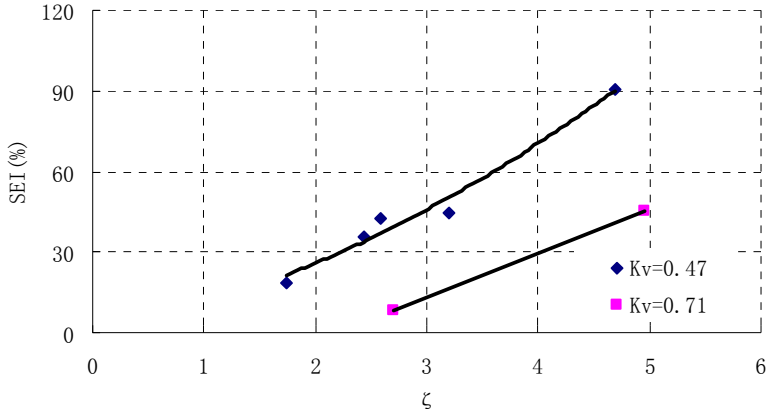

Fig. 6 The percentage increase of carrying capacity SEI versus confinement factor ζ

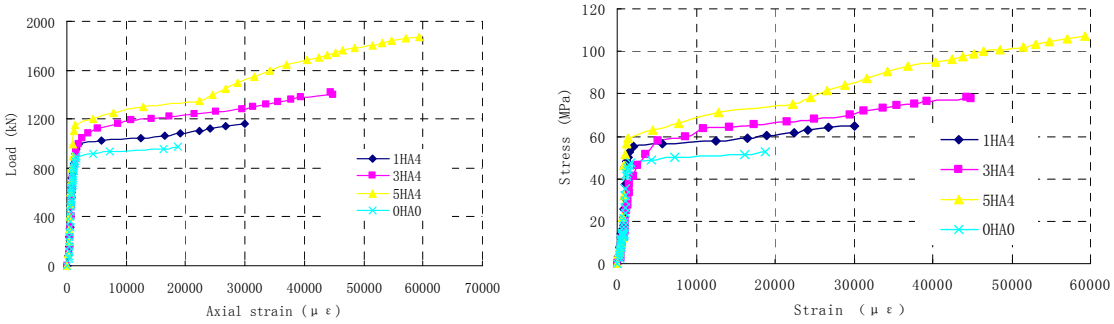

(a) (b)

Fig. 7 Effect of FRP wall thickness on specimen strains: (a) Load-strain curves of specimens; (b) Stress-strain curves of confined concretes

load-strain curve. In the initial stage of deformation, the axial load-strain curves of specimens with different FRP wall thicknesses have almost the same slope, and the axial stress-strain response ofconfined concrete follows the path of unconfined concrete. Afterwards, the FRP jacket and the steel tubes are fully activated by the further increasing load. And the fibres in the hoop direction begin to resist the transverse expansion of the outer steel tube, thus provide a confining pressure to concrete core together with steel tubes. Indeed, the carrying capacities of specimens 1HA4, 3HA4 and 5HA4 were, respectively, 18%, 45% and 91% larger than that of specimen 0HA0, along with the increases of 24%, 49% and 103% in the strength of confined concrete.

Fig. 8(a) compares the axial load-strain relationship among specimens with different hollow section ratios (i.e., 3SA4, 3HA4 and 3HB4). It is seen from Fig. 8(a) that all the axial load-strain curves in the initial stage of the deformation have almost the same slope, while in the following stage, the slopes of the curves and the carrying capacities of the columns increase with the decrease of the hollow section ratio. It could be seen from Fig. 8(b) that the hollow section ratio has no significant influence on the axial stress-strain relationship of concrete. The stress-strain curve for 3HA4 followed almost the same path as that for 3SA4 up to failure. This means that the

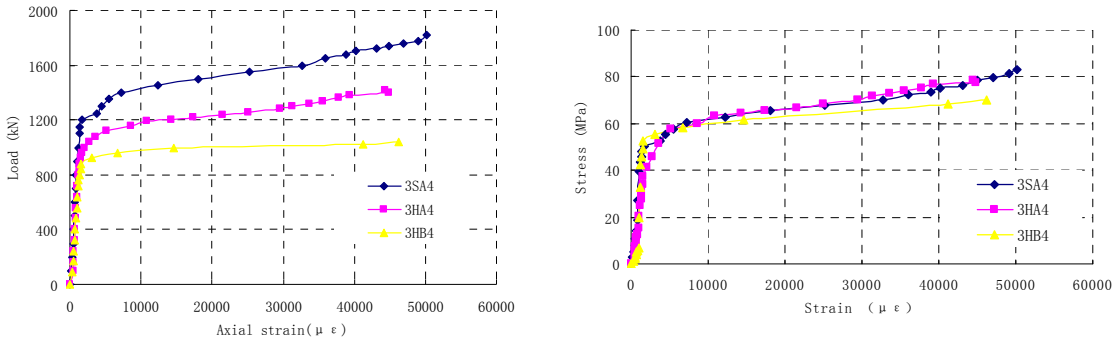

(a) (b)

Fig. 8 Effect of hollow section ratio on specimen strains: (a) Load-strain curves of specimens; (b) Stress-strain curves of confined concrete

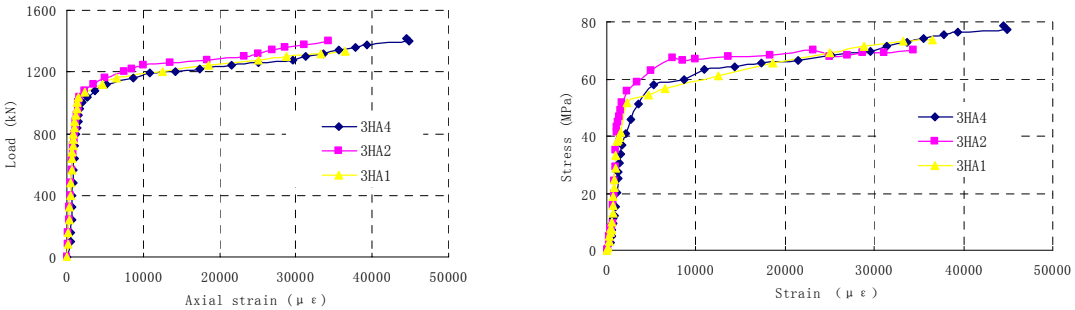

(a) (b)

Fig. 9 Effect of fibre longitudinal-circumferential proportion on specimen strains: (a) Load-strain curves of specimens; (b) Stress-strain curves of concrete

confinement effect of the concrete in the column with hollow section ratio 0.47 was similar to that in a solid circular column. As a result, the carrying capacities of specimens 3SA4 and 3HA4 were, respectively, 75% and 37% larger than that of specimen 3HB4, along with the increases of 18.5% and 12% in strength of confined concrete.

The axial load-strain and concrete stress-strain responses of the specimens with different fibre longitudinal-circumferential proportions (3HA1, 3HA2 and 3HA4) are given in Fig. 9. It is shown from Fig. 9 that stiffnesses and confinement effects of these columns are similar each other. This indicates that the fibre longitudinal-circumferential proportion has little influence on the axial behaviour of CFDST stub columns confined by FRP.

2.4.3 Failure modes

Failure of the CFDST specimens was typically initiated by a local buckling on the middle portion of the outer tubes, and a local buckling of the inner tubers also occurred as shown in Figs. 3(a) and 4(a). Failure of the CFDST specimens confined by FRP was initiated by sudden rupture of the FRP jackets followed by buckling of the steel tubes, and it exhibited higher hoop deflection for specimens with more FRP layers, as shown in Figs. 3(b)-(d). Failure of the CFST specimens

confined by FRP was similar with CFDST specimens confined by FRP, as shown in Fig. 4(d). All steel tubes strengthened by FRP buckled later than the un-strengthened ones.

3. Strength model of confined concrete

When concrete is subjected to laterally confining pressure, the uniaxial compressive strength f_{cc} is much higher than those of unconfined concrete. Lam and Teng (2003) suggested that the compressive strength of the FRP-confined concrete is expressed as a function of the lateral confining pressure using the following relationship

$$\frac{f_{cc}}{f'_{co}} = 1 + 3.3\frac{f_l}{f'_{co}} \tag{6}$$

where f_l is lateral confining pressure of FRP.

For CFDST columns, Hu and Su (2011) used following equation to estimate the confined concrete strength.

$$\frac{f_{cc}}{f'_{co}} = 1 + 4.1\frac{f_{sl}}{f'_{co}} \tag{7}$$

where f_{sl} is lateral confining pressure of outer steel tube.

For CFST columns confined by FRP, Park *et al.* (2011) used following equation to estimate the confined concrete strength

$$\frac{f_{cc}}{f'_{co}} = 1 + 2.86\frac{f_l}{f'_{co}} \tag{8}$$

In this section, an empirical model is proposed to calculate the concrete strengths of CFSDT columns confined by FRP, CFDST columns as well as CFST columns confined by FRP. The effects of confinement factor ζ_f, hollow section ratio K_v and lateral confining pressure of outer steel tube f_{sl} are considered in predicting the compressive strength of confined concrete f_{cc} as follows

$$\frac{f_{cc}}{f'_{co}} = 1 + 1.2\zeta_f\left(1 - 0.85K_v\right) + 3.2\sqrt{\frac{f_{sl}}{f'_{co}}\left(1 - K_v\right)} \tag{9}$$

The proposed formula is built on the basis of the available experimental data. In Table 4, the values of confined concrete strength from Eq. (9) are compared with the experimental values f^e_{cc} obtained from the measurement data. The mean value of f_{cc}/f^e_{cc} is 1.013 and the mean squared deviation of f_{cc}/f^e_{cc} is 0.0703. This means that the confined concrete strength from the proposed formula matches well with the experimental one.

4. Prediction of carrying capacity

In this section, the carrying capacity of CFDST stub columns confined by FRP is analyzed, based on the following assumptions:

Table 4 Comparison of confined concrete strength from theoretical analysis and experimental measurement

Specimen	$\frac{f_{cc}}{f'_{co}}$ [a]	$\frac{f^e_{cc}}{f'_{co}}$ [b]	$\frac{f_{cc}}{f^e_{cc}}$
3SA4	4.94	4.42	1.12
0HA0	2.58	2.80	0.92
1HA4	3.14	3.46	0.91
3HA4	4.18	4.18	1.00
3HA2	3.77	3.74	1.01
3HA1	3.63	3.52	1.03
5HA4	5.51	5.69	0.97
0HB0	2.48	2.32	1.07
1HB4	2.99	2.78	1.08
3HB4	3.95	3.73	1.06

[a] f_{cc} is the compressive strength of confined concrete from Eq. (9) and f'_{co} is taken as 67% of the compression strength of cubic blocks .

[b] f^e_{cc} is the compressive strength of confined concrete from test data.

(1) Since the compressive strength and modulus of FRP jacket in the axial direction are much less than the tensile strength and modulus in the hoop direction, the axial compressive capacity of FRP jacket is ignored in the analysis. Namely, only the hoop confinement of FRP is considered.
(2) The steel tube in the CFDST columns confined by FRP is relatively thin, therefore the radial direction stress of the steel tube is negligible, comparing to the stresses in other two directions. Moreover, the von-Mises' yield criterion for steel under biaxial stress state is adopted.
(3) When the concrete is subjected to laterally confining pressure, the axial compressive strength is much higher than that of the unconfined concrete. Eq. (9) is used here to determine the compressive strength of concrete confined by FRP jacket and steel tubes.
(4) The interactions among FRP jacket, steel tube and filled-in-concrete are assumed to be no separation when loading.

Based on the above assumptions, the entire applied load on the composite columns should be the summation of the loads on filled-in-concrete, outer steel tube and inner steel tube. Fig. 10 shows the equilibrium relationship among three kinds of materials. According to the equilibrium condition, the ultimate axial force $N_{u,fs}$ can be expressed as

$$N_{u,fs} = f_{cc}A_c + \sigma_{o1}A_{s1} + \sigma_{i1}A_{s2} \tag{10}$$

$$2\sigma_{o2}t_{s1} = p_{s1}D_{oc} \tag{11}$$

$$2\sigma_{i2}t_{s2} = -p_{s2}D_i \tag{12}$$

where σ_{o1} is the longitudinal stress of outer steel tube, σ_{o2} is the circumferential stress of outer steel

tube, σ_{i1} is the longitudinal stress of inner steel tube, σ_{i2} is the circumferential stress of inner steel tube, A_{s2} is the cross-sectional area of the inner steel tube, p_{s2} is the lateral confining stress of inner steel tube, D_{oc} is the outsider diameter of concrete, and t_{s2} is the wall thickness of inner steel tube.

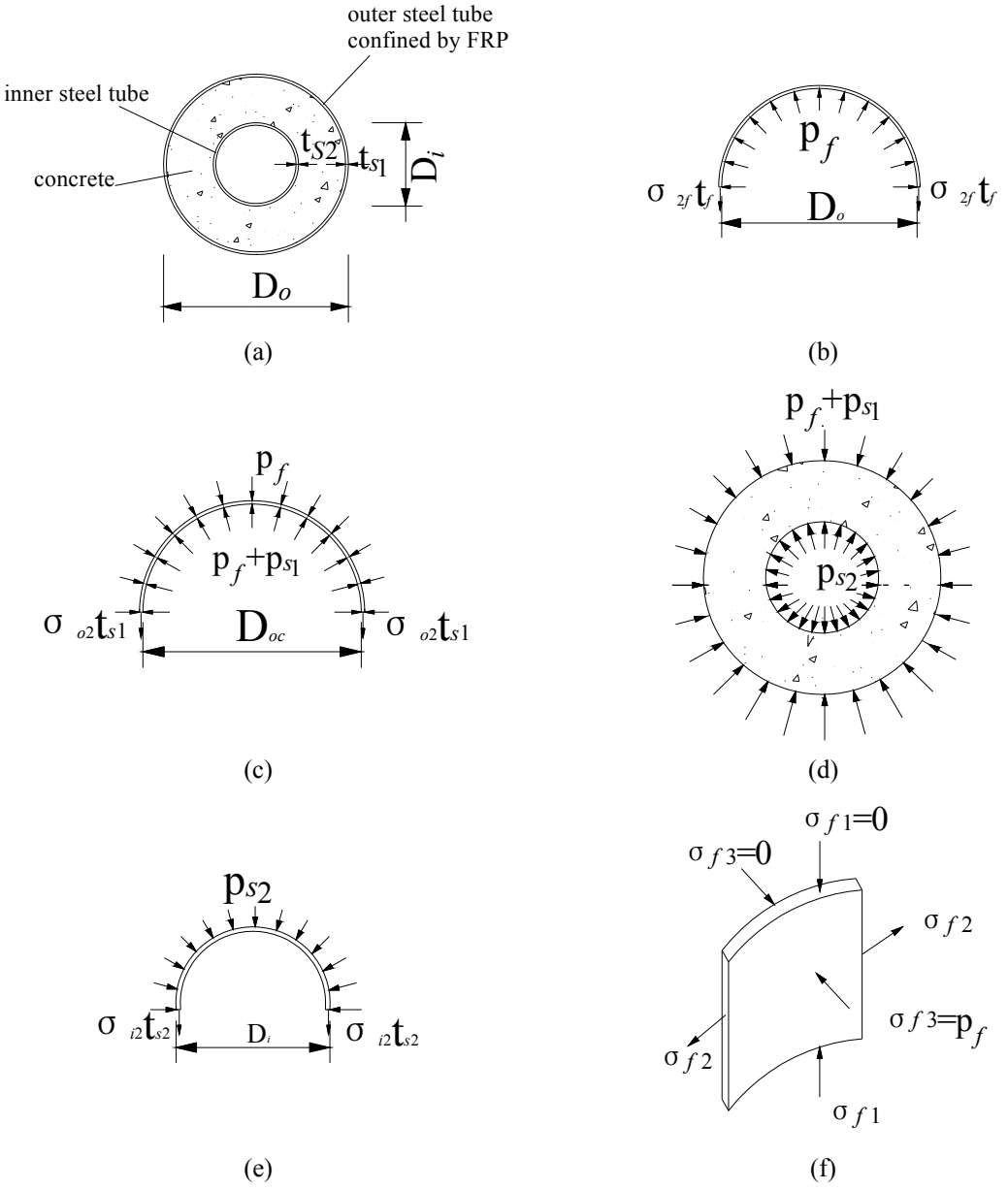

Fig. 10 Stress diagram of the composite section: (a) Cross section of composite column; (b) Stress diagram of GFRP; (c) Stress diagram of outer steel; (d) Stress diagram of confined concrete; (e) Stress diagram of inner steel; (f) Micro-element stress diagram of GFRP wall; (g) Micro-element stress diagram of outer steel tube wall; (h) Micro-element stress diagram of inner steel tube wall

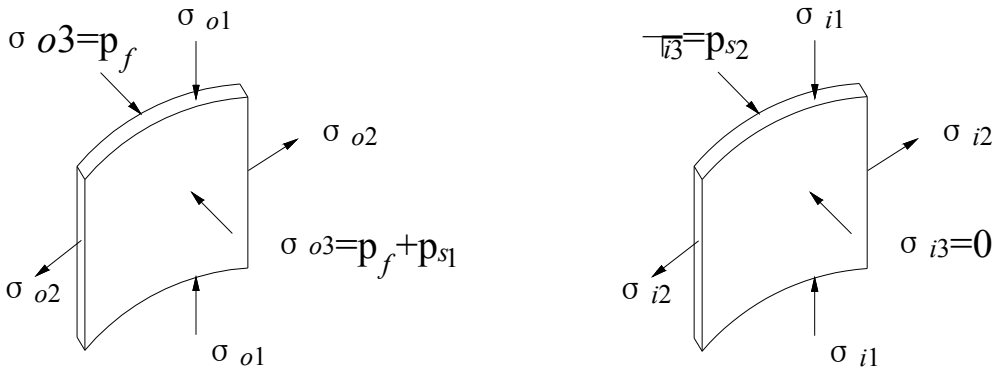

(g) (h)

Fig. 10 Continued

The longitudinal stresses of outer and inner steel tubes can be obtained from the von-Mises' yield criterion

$$\sigma_{o1} = \sqrt{f_{yo}^2 - 3p_{s1}^2\left(\frac{A_c}{A_{s1}}\right)^2} - \frac{p_{s1}A_c}{A_{s1}} \tag{13}$$

$$\sigma_{i1} = \sqrt{f_{yi}^2 - 3p_{s2}^2\left(\frac{A_c}{A_{s2}}\right)^2} - \frac{p_{s2}A_c}{A_{s2}} \tag{14}$$

where f_{yi} is the yield strength of inner steel tube.

Going with the increase of the axial load on the column, the concrete gradually dilated and expanded laterally. The lateral confining stress (p_{s2}) is shown to be negative. This means the inner steel tube has a tendency to buckling to the centre of the circle column. In such a case, the confining stress provided by inner steel tube can be ignored

$$p_{s2} \approx 0 \tag{15}$$

Now, substituting Eq. (15) into Eqs. (12) and (14), the longitudinal stress of inner steel tube under the ultimate equilibrium condition was obtained

$$\sigma_{i1} = f_{yi} \tag{16}$$

Substituting Eqs. (9), (13) and (16) into Eq. (10), the carrying capacity N is

$$\begin{aligned} N_{u,fs} = {} & A_c f'_{co}\left[1 + 1.2\xi\left(1 - 0.85K_v\right) + 3.2\sqrt{\frac{p_{s1}}{f_{ck}}\left(1 - K_v\right)}\right] \\ & + A_{s1}\left[\sqrt{f_{yo}^2 - 3p_{s1}^2\left(\frac{A_c}{A_{s1}}\right)^2} - \frac{p_{s1}A_c}{A_{s1}}\right] + A_{s2}f_{yi} \end{aligned} \tag{17}$$

The first derivative of Eq. (17) with respect to p_{s1} taking zero can determine the local extremum

$$\frac{dN_{u,fs}}{dp_{s1}} = 0 \tag{18}$$

Therefore, p_{s1} corresponding to the carrying capacity $N_{u,fs}$ is

$$1.6A_c\sqrt{\frac{f_{co}^{'}(1-K_v)}{p_{s1}}} - \frac{A_{s1}D_{oc}}{4t_{s1}}\left[\frac{3D_{oc}p_{s1}}{\sqrt{16t_{s1}^2f_{yo}^2 - 3D_{oc}^2p_{s1}^2}} + 1\right] = 0 \tag{19}$$

Finally, $N_{u,fs}$ can be obtained by substituting p_{s1} back into Eq. (17).

Taking $K_v = 0$ and $A_{s2} = 0$, the carrying capacities of CFST stub columns confined by FRP can be obtained directly from Eqs. (19) and (17) and taking $\zeta_f = 0$, the carrying capacities of CFDST stub columns can be obtained.

Table 5 gives the comparison of the predicted $N_{u,fs}$ obtained from Eq. (19) and Eq. (17) with $N_{u,fs}^*$ obtained from the experiment. The mean value of $N_{u,fs}/N_{u,fs}^*$ is 1.009 and the mean squared deviation of $N_{u,fs}/N_{u,fs}^*$ is 0.081. Table 6 gives the comparison of the predicted $N_{u,f}$ of CFST stub columns confined by FRP with $N_{u,f}^*$ from the experimental results of Wang *et al.* (2005a). The mean value of $N_{u,f}/N_{u,f}^*$ is 1.026 and the mean squared deviation is 0.0033. Table 7 gives the comparison of the predicted $N_{u,s}$ of CFDST stub columns with $N_{u,s}^*$ from the experimental results of Tao *et al.* (2004) and Zhao *et al.* (2002). The mean value of $N_{u,s}/N_{u,s}^*$ is 1.023 and the mean squared deviation is 0.007. It could be seen from Tables 5-7 that the predicted results agree well with the experimental ones.

Table 5 Comparisons of predicted carrying capacity and experimental results

Specimen	A_c (mm^2)	A_{s1} (mm^2)	A_{s2} (mm^2)	$N_{u,fs}$ (kN)	$\frac{N_{u,fs}}{N_{u,fs}^*}$ [a]
3SA4	20499.93	871.7	0	1963.12	1.079
0HA0	15965.77	871.7	281.85	942.12	0.961
1HA4	15965.77	871.7	281.85	1097.54	0.946
3HA4	15965.77	871.7	281.85	1413.39	0.995
3HA2	15965.77	871.7	281.85	1279.36	0.914
3HA1	15965.77	871.7	281.85	1249.09	0.938
5HA4	15965.77	871.7	281.85	1735.49	0.928
0HB0	10298.07	871.7	599.46	792.83	1.109
1HB4	10298.07	871.7	599.46	897.05	1.156
3HB4	10298.07	871.7	599.46	1107.35	1.065

[a] $N_{u,fs}$ is the predicted carrying capacity of the tested columns obtained from proposed formulas and $N_{u,fs}^*$ is the carrying capacity of the columns obtained from the test.

Notes: A_c is the cross-sectional area of concrete, A_{s1} is the cross-sectional area of outer steel tube, A_{s2} is the cross-sectional area of inner steel tube.

Table 6 Comparison of axial carrying capacity of CFST stub columns confined by FRP from theoretical analysis and experimental results

Specimen[a]	f'_{co} (Mpa)	f_y (Mpa)	f_{cc} (Mpa)	D_{oc} (mm)	D_o (mm)	t_{s1} (mm)	t_{cf} (mm)	$N_{u,f}$ (kN)	$N^*_{u,f}$ (kN)	$\frac{N_{u,f}}{N^*_{u,f}}$ [b]
0-6.0	35.51	350	120.83	124	136	6.0	0	1964.91	1844.4	1.07
1-4.5	36.85	310	122.03	124	133	4.5	0.167	1733.80	1698.3	1.02
1-6.0	35.51	350	128.26	124	136	6.0	0.167	2054.55	1939.4	1.06
2-3.5	36.85	310	123.78	124	131	3.5	0.334	1659.74	1592.5	1.04
2-4.5	36.85	310	129.62	124	133	4.5	0.334	1825.46	1846.3	0.99
2-6.0	35.51	350	135.68	124	136	6.0	0.334	2144.19	2186.4	0.98

[a] In the first column, the first number means the layer number of CFRP and the last number means the thickness of steel tube.

[b] $N_{u,f}$ is the predicted carrying capacity of CFST stub columns confined by FRP obtained from proposed formulas and $N^*_{u,f}$ is the experimental results of Wang *et al*. (2005a)

Note: f'_{co} is taken as 67% of the compression strength of cubic blocks, f_y is the yield strength of steel tube, f_{cc} is confined concrete strength calculated from Eq. (9), D_{oc} is the outsider diameter of concrete, D_o is the outside diameter of steel tube, t_{s1} is the wall thickness of steel tube, t_{cf} is the wall thickness of CFRP jacket.

Table 7 Comparison of axial carrying capacity of CFDST stub columns from theoretical analysis and experimental results

Specimen[a]	$\frac{f_{cc}}{f'_{co}}$	$N_{u,s}$ (kN)	$N^*_{u,f}$ (kN)	$\frac{N_{u,f}}{N^*_{u,f}}$ [b]
CC2a	2.03	1807	1800	1.00
CC3a	1.67	1574	1665	0.95
CC5a	1.72	828	915	0.91
CC6a	1.63	2379	2430	0.98
CC7a	1.37	3030	3330	0.91
C1C7	1.83	1693	1418	1.19
C2C7	1.75	1417	1390	1.02
C3C7	1.75	1312	1191	1.10
C4C7	1.63	1107	1100	1.01
C5C8	1.30	1884	1700	1.11
C6	1.30	1702	1591	1.07

[a] In the first column, the first number means the layer number of CFRP and the last number means the thickness of steel tube.

[b] $N_{u,s}$ is the predicted carrying capacity of CFDST stub columns obtained from proposed formulas and $N^*_{u,f}$ is the experimental results of Tao *et al*. (2004) and Zhao *et al*. (2002).

Note: f'_{co} is taken as 67% of the compression strength of cubic blocks, and f_{cc} is confined concrete strength calculated from Eq. (9).

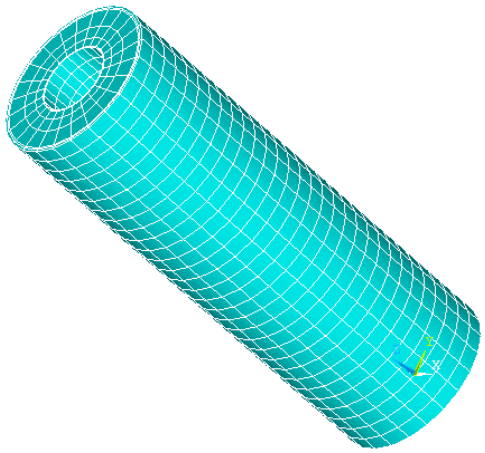

Fig. 11 Finite element mesh for CFDST columns confined by FRP

5. Finite element analysis

The accuracy of concrete strength model and prediction of carrying capacity of CFDST stub columns confined by FRP is further examined by FE model analysis.

5.1 FE model

A three dimension FE model has been developed for the nonlinear analysis of CFDST stub columns confined by FRP under axial loading, and typical FE meshes are shown in Fig. 11. The bottom surface of columns was assumed to be fixed, and the lateral displacement of upper and lower bounds are restrained to prevent the elephant foot buckling. A uniform distributed load was applied incrementally at the top surface of the column using the displacement control approach. The finite element model consisted of two types of elements: SOLID186 for steel tubes and FRP jackets and SOLID45 for concrete.

In this model, the FRP was assumed to behave in a linear elastic manner both in the longitudinal and the circumferential directions. The stresses in the FRP jacket are expressed as (Bank 2006 and Kian *et al.* 2011)

$$\sigma_{f1} = \frac{E_{f1}}{1 - v_{12}v_{21}}\varepsilon_{f1} + \frac{v_{12}E_{f1}}{1 - v_{12}v_{21}}\varepsilon_{f2} \tag{20}$$

$$\sigma_{f2} = \frac{v_{21}E_{f2}}{1 - v_{12}v_{21}}\varepsilon_{f1} + \frac{E_{f2}}{1 - v_{12}v_{21}}\varepsilon_{f2} \tag{21}$$

where σ_{f1} and σ_{f2} are the longitudinal and circumferential stresses in the FRP jacket, respectively, and ε_{f1} and ε_{f2} are the corresponding strains. E_{f1} and E_{f2} are the longitudinal compressive and circumferential tensile moduli of the FRP jacket, respectively, and v_{21} and v_{12} are Poisson's ratios corresponding to loading in longitudinal and circumferential directions, respectively.

Moreover, in predicting the carrying capacity, it was assumed that failure occurs due to rupture

of the FRP jackets. The Tsai-Wu criterion was used to evaluate the failure of FRP

$$\left(\frac{1}{S_{2,t}}-\frac{1}{S_{2,c}}\right)\sigma_{f2u}+\left(\frac{1}{S_{1,t}}-\frac{1}{S_{1,c}}\right)\sigma_{f1u} + \frac{1}{S_{2,t}S_{2,c}}\sigma_{f2u}^2+\frac{1}{S_{1,t}S_{1,c}}\sigma_{f1u}^2-\frac{1}{\sqrt{S_{1,c}S_{1,t}S_{2,t}}}\sigma_{f2u}\sigma_{f1u}=1 \tag{22}$$

where $S_{1,c}$ and $S_{2,c}$ are the longitudinal and circumferential compressive strength of the FRP jacket, respectively, $S_{1,t}$ and $S_{2,t}$ are the longitudinal and circumferential tensile strength respectively, and σ_{f1u} and σ_{f2u} are the ultimate state of longitudinal and circumferential stress of the FRP jacket.

The steel tube was assumed to be an elastic-plastic material with a strain-hardening behavior from the yield to the ultimate stress. As shown in Fig. 12, the confined concrete core was modeled based on the constitutive relationship proposed by Lam and Teng (2003)

$$\sigma_c=\begin{cases}E_c\varepsilon_c-\dfrac{(E_c-E_2)^2}{4f_{co}^{'}}\varepsilon_c^2 & (0\le\varepsilon_c\le\varepsilon_t)\\ f_{co}^{'}+E_2\varepsilon_c & (\varepsilon_t\le\varepsilon_c\le\varepsilon_{cc})\end{cases} \tag{23}$$

where σ_c and ε_c are the axial stress and strain of the confined concrete, respectively, E_c is the elastic modulus of the unconfined concrete, E_2 is the slope of the linear branch, and ε_t is the transition axial strain at the intersection of the linear and parabolic branches, which can be expressed as

$$\varepsilon_t=\frac{2f_{co}'}{E_c-E_2} \tag{24}$$

Eq. (9) for calculating f_{cc} and a formula proposed by Lam and Teng (2003) for calculating the ultimate strain ε_{cc} were adopt in this model

$$\frac{\varepsilon_{cc}}{\varepsilon_{co}}=1.75+12\left(\frac{f_l}{f_{co}^{'}}\right)\left(\frac{\varepsilon_{lu}}{\varepsilon_{co}}\right)^{0.45} \tag{25}$$

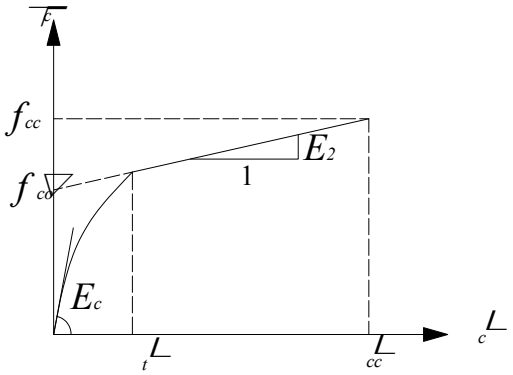

Fig. 12 The stress-strain relationship for confined concrete under axial compression

where ε_{co} is the lateral strain at FRP rupture.

The FE model was also used to investigate the behaviour of CFDST stub columns under axial loading, and the von-Mises' yield criterion is adopted to predict yielding of steel tubes.

5.2 Comparison between the proposed formulas with FE analysis results

The developed FE model was employed to simulate the behaviour of tested columns. Fig. 13 shows a comparison of numerical and measured axial load-strain curves for CFDST stub columns

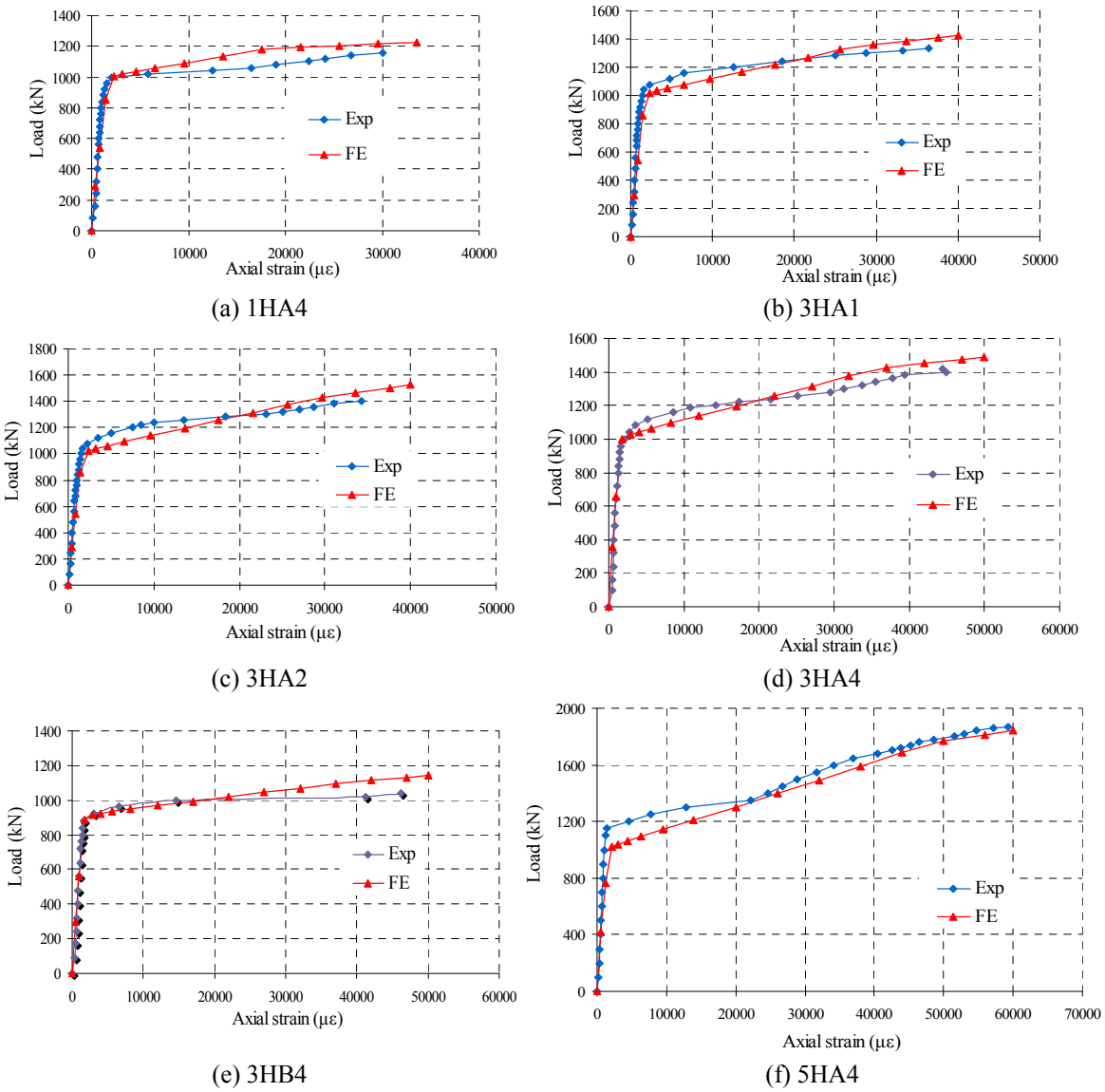

Fig. 13 Comparisons of numerical and test axial load-strain curves for CFDST stub columns confined by FRP

Table 8 Results of FE analysis

Specimen	$N_{u,fs}^{F}$ (kN)	$\frac{N_{u,fs}^{F}}{N_{u,fs}^{*}}$ [a]	$\frac{N_{u,fs}}{N_{u,fs}^{F}}$ [b]
3SA4	1949	1.07	1.01
0HA0	1073	1.09	0.88
1HA4	1224	1.06	0.90
3HA4	1491	1.05	0.95
3HA2	1524	1.09	0.84
3HA1	1428	1.07	0.87
5HA4	1840	0.98	0.94
0HB0	823	1.16	0.96
1HB4	924	1.19	0.97
3HB4	1142	1.10	0.97

[a] $N_{u,fs}^{F}$ is the carrying capacity of the tested columns from FE analysis and $N_{u,fs}^{*}$ is the carrying capacity of the columns obtained from the experiment.

[b] $N_{u,fs}$ is the predicted carrying capacity of the tested columns obtained from the proposed formulas.

confined by FRP. It appears that the FE model predicts very well the axial stiffness, the carrying capacity and the post-peak behaviour of the axial load-strain curves for the tested columns. Table 8 gives the comparison of predicted carrying capacity $N_{u,fs}^{F}$ obtained from FE analyses with tested data $N_{u,fs}^{*}$. The mean value of $N_{u,fs}^{F}/N_{u,fs}^{*}$ is 1.09 with the mean squared deviation of 0.0029. Then, the predicted carrying capacity $N_{u,fs}$ obtained from proposed formulas is compared with $N_{u,fs}^{F}$ in Table 8. The mean value of $N_{u,fs}/N_{u,fs}^{F}$ is 0.93 with the mean squared deviation of 0.0026. The results of proposed formulas are found to be in good agreement with the FE analysis values.

6. Conclusions

Using FRP confinement to enhance the axial compressive behaviour of CFSDT columns has been explored. A series of axial compression tests have been made to study the effectiveness of FRP confinement on CFSDT columns. Based on the results from the present analytical procedures, the following conclusions are obtained:

(1) Both the load-strain curve for specimen and stress-strain curve for confined concrete behave bilinearly. In the first stage of loading, the concrete is known to behave elastically and the strain is related proportionally to the axial load. As the load further increases, cracks gradually form in concrete. This leads to a large increase in transverse strain which activates the FRP jacket and steel tube to resist the transverse expansion. So the curves at the second stage of loading are still up. The slope of the curve depends on the geometry of the cross-section and the confinement factors. It is observed that all specimens confined by FRP have a considerable increase in carrying capacities over the specimens without FRP.

(2) The effects of various parameters on the specimen performance under axial loading are

discussed in detail. It is found that the FRP wall thickness not only influences the carrying capacities of CFDST stub columns confined by FRP, but also influences the strength of confined concrete. The hollow section ratio has little influence on the axial stress-strain relationship of concrete. The confinement effects of concrete in void column with hollow section ratio 0.47 are similar to that in the circular solid column. Moreover, the fibre longitudinal-circumferential proportion has no significant influence on the axial behaviour of CFDST stub columns confined by FRP.

(3) A model for predicting the strength of confined concrete is developed on the basis of the available experimental data. The effects of confinement factor, hollow section ratio and lateral confining pressure of outer steel tube are considered in the model which can be used as a basis for the prediction of the carrying capacities of CFDST stub columns confined by FRP.

(4) The proposed formula for predicting the carrying capacity has been proved to be effective by the experimental results and FE analysis. The formula can also be applied to calculate the carrying capacities of CFDST stub columns and CFST stub columns confined by FRP.

Acknowledgments

The financial supports from National Natural Science Foundation of China (51308288), National Key Basic Research Program of China (973 Program, Grant No.2012CB026205), Key Program of National Natural Science Foundation of China (51238003), University Science Research Project of Jiangsu province, China (11KJB560002) and Jiangsu Government Scholarship for Overseas Studies (JS-2013-184) are highly appreciated.

References

Bank, L.C. (2006), *Composites for Construction*: *Structural Design with FRP Materials*, John Wiley & Sons.

Furlong, R.W. (1967), "Strength of steel-encased concrete beam–columns", *J. Struct. Div.*, **93**(5), 113-125.

Haedir, J., Zhao, X.L., Bambach, M.R. and Grzebieta, R.H. (2010), "Analysis of CFRP externally-reinforced steel CHS tubular beams", *Compos. Struct.*, **92**(12), 2992-3001.

Han, L.H., Huang, H. and Zhao, X.L. (2009), "Analytical behaviour of concrete-filled double skin steel tubular (CFDST) beam-columns under cyclic loading", *Thin-Wall. Struct.*, **47**(6-7), 668-680.

Hu, H.T. and Su, F.C. (2011), "Nonlinear analysis of short concrete-filled double skin tube columns subjected to axial compressive forces", *Marine Struct.*, **24**(4), 319-337.

Jiao, H. and Zhao, X.L. (2004), "CFRP strengthened butt-welded very high strength (VHS) circular steel tubes", *Thin-Wall. Struct.*, **42**(7), 963-978.

JTS 153-3-2007 (China Code) (2007), Technical Specification for Corrosion Protection of Steel Structures for Sea Port Construction, Ministry of Transport of the People's Republic of China.

Karimi, K., Tait, M.J. and EI-Dakhakhni, W.W. (2011), "Testing and modeling of a novel FRP-encased steel –concrete composite column", *Compos. Struct.*, **93**(5), 1463-1473.

Knowles, R.B. and Park, R. (1969), "Strength of concrete-filled steel tubular columns", *J. Struct. Div.*, **95**(12), 2565-2587.

Lam, L. and Teng, J.G. (2003), "Design-oriented stress-strain models for FRP-confined concrete", *Construct. Build. Mater.*, **17**(6), 471-489.

Miller, T.C., Chajes, M.J., Mertz, D.R. and Hastings, J.N. (2001), "Strengthening of a steel bridge girder using CFRP plates", *J. Bridge Eng.*, **6**(6), 514-522.

Montague, P. (1978), "The experimental behaviour of double-skinned, composite, circular cylindrical shells under external pressure", *J. Mech. Eng. Sci.*, **20**(1), 21-34.
Nie, J.G. and Liao, Y.B. (2008), "Bearing capacity calculations for concrete filled double skin tubes", *J. Tsinghua Univ. (Sci. & Tech.)*, **48**(3), 312-315. [In Chinese]
Nishino, T. and Furukawa, T. (2003), "Strength and deformation capacities of circular hollow section steel member reinforced with carbon fiber", *J. Struct. Eng., B*, **49B**, 489-496.
Park, J.W., Hong, Y.K., Hong, G.S., Kim, J.H. and Choi, S.M. (2011), "Design formulas of concrete filled circular steel tubes reinforced by carbon fiber reinforced plastic sheets", *Procedia Eng.*, **14**, 2916-2922.
Schnerch, D. and Rizkalla, S. (2004), "Strengthening of scaled steel-concrete composite girders and steel monopole towers with CFRP", FRP Composite in Civil Engineering, Taylor & Francis Group, London, UK.
Seica, M.V. and Packer, J.A. (2007), "FRP materials for the rehabilitation of tubular steel structures, for underwater applications", *Compos. Struct.*, **80**(3), 440-450.
Sen, R. and Liby, L. (1994), "Repair of steel composite bridge sections using carbon fiber reinforced plastic laminates, U.S", Department of Transportation Contract B-7932; University of South Florida, Tampa, FL, USA.
Shaat, A. and Fam, A. (2006), "Axial loading tests on CFRP-retrofitted short and long HSS steel columns", *Can. J. Civil Eng.*, **33**(4), 458-470.
Tao, Z., Han, L.H. and Zhao, X.L. (2004), "Behaviour of concrete-filled double skin (CHS inner and CHS outer) steel tubular stub columns and beam-columns", *J. Construct. Steel Res.*, **60**(8), 1129-1158.
Tao, Z., Han, L.H. and Wang, L.L. (2007), "Compressive and flexural behaviour of CFRP-repaired concrete-filled steel tubes after exposure to fire", *J. Construct. Steel Res.*, **63**(8), 1116-1126.
Tao, Z., Han, L.H. and Zhuang, J.P. (2008), "Cyclic performance of fire-damaged concrete-filled steel tubular beam–columns repaired with CFRP wraps", *J. Construct. Steel Res.*, **64**(1), 37-50.
Teng, J.G. and Hu, Y.M. (2007), "Behaviour of FRP-jacketed circular steel tubes and cylindrical shells under axial compression", *Construct. Build. Mater.*, **21**(4), 827-838.
Teng, J.G., Yu, T., Wong, Y.L. and Dong, S.L. (2007), "Hybrid FRP-concrete-steel tubular columns: Concept and behavior", *Construct. Build. Mater.*, **21**(4), 846-854.
Wang, Q.L., Wu, W. and Zhao, Y.H. (2005a), "An experimental study on concentrically concrete circular CFRP-steel composite tubular stub columns", *China Civil Eng. J.*, **38**(10): 44-48. [In Chinese]
Wang, Q.L., Zhao, C.L., Zhang, H.B. and Zhang, Y.D. (2005b), "The simplified calculation of bearing capacity on concentrically concrete circular CFRP-steel composite tubular stub columns", *J. Shenyang Jianzhu Univ. (Natural Science, China),* **21**(6), 612-615. [In Chinese]
Zhao, X.L. and Zhang, L. (2007), "State-of the-art review on FRP strengthened steel structures", *Eng. Struct.*, **29**(8), 1808-1823.
Zhao, X.L., Grzebieta, R.H. and Elchalakani, M. (2002), "Tests of concrete-filled double skin CHS composite stub columns", *Steel Compos. Struct., Int. J.*, **2**(2),129-146.

CC